Real-time implementation of a combined controller-observer approach for shunt active filters

Nagulapati Kiran[1,2], I. E. S. Naidu[1]

[1]Department of Electrical, Electronics, and Communication Engineering, GITAM Deemed to be University, Visakhapatnam, India
[2]Department of Electrical and Electronics Engineering, Anil Neerukonda Institute of Technology and Sciences (ANITS), Visakhapatnam, India

ABSTRACT

The crucial role of shunt active power filter (SAPF) is to compensate for reactive power, balances unbalanced currents and counteract harmonics produced due to non-linear loads, by injecting phase-opposed compensation current by designing an appropriate controller. In this work, a combined controller-observer state and disturbances estimation scheme for a SAPF is proposed. To avoid the requirement of full-state feedback, unknown input observers (UIO) is designed. This is conducted in OPAL-RT OP4510 environment. Real-time simulations are used to show how successful the suggested controller-observer architecture for SAPF is; wherein the estimated states from the observer are fed back to the controller, and finally, the disturbance is also estimated. UIO is designed for SAPF to deal with nominal conditions and in the presence of sinusoidal disturbance.The OPAL-RT results clearly show that LO introduces steady state error between the reference input and the estimated state of SAPF in the presence of disturbances. This steady state error is completely eliminated in presence of all disturbances using UIO. The results also show that UIO perfectly tracks the reference input in the presence of disturbances. Further, disturbances are also estimated perfectly with UIO.

Corresponding Author:

I. E. S. Naidu
Department of Electrical, Electronics, and Communication Engineering, GITAM Deemed to be University
Visakhapatnam, India
Email: ninjarap@gitam.edu

1. INTRODUCTION

Power quality has a significant role to play in power systems. The recent inception of grids of smart technology apprehends the significance of the quality of power. Industries incur drastic losses every year throughout the world, as they are unable to provide quality power. The desiring factor in the power sector industry is to draw a disturbance-free sinusoidal current, which is a huge mountain to achieve in today's scenario because of the use of increasing power electronics converters. The concept of harmonic mitigation has led to many compensation methods as well as many topologies. Shunt passive filter has paved a way for compensating current harmonics in alternating current (AC) networks, but with complications such as variation of source impedance with the system, anti-resonance phenomenon between source impedance and filter, and overloading of filter, thereby increasing harmonics in current. These realistic problems in power systems have drawn considerable attention in the power system research community. These limitations can be overcome by using active power filters (APFs), which can compensate for harmonics and avoid many of the problems. Many researchers

have done extensive work on shunt active power filter (SAPF). Simulation of SAPF and design aspects were presented in [1], where the results of the experimental prototype developed using a micro-controller-based system were effectively designed, bringing source current's total harmonic distortion (THD) down to less than 5 percentage. Akagi *et. al.* [2] compared various current control methods such as digital current control, proportional control, and deadbeat control have been designed for a three-phase three-wire SAPF. Depending upon the type of converter and topology being utilized, various control strategies have been designed for three-phase four-wire SAPF. Kedjar and Al-Haddad [3] proposed a DSP-based LQR controller with integral action (LQRI) is implemented for SAPF, which eliminates steady-state errors to achieve tracking of reference and regulate direct current (DC) bus voltage. Jarou *et al.* [4] explained a novel control rule based on approximated state feedback utilizing a Luenberger observer (LO) to enhance the stability and dynamics of SAPF.

Benchouia *et al.* [5] presented a comparative simulation, as well as experimental analysis, wherein the sliding mode control (SMC) offers improved outcomes when compared to PI controller. The charging stations of electric vehicles are equipped with SAPF in order to eliminate the problem of propagation of current distortions into the grid. Ali *et al.* [6] presented a comparative analysis for SAPF using PI and artificial neural network (ANN) controllers to improve power quality is presented in [6]. The categorization and classification of APFs are detailed in [7]; based on various factors including circuit configuration, mitigation purposes, and control strategies. Shukla *et al.* proposed a real-time implementation of an online empirical mode decomposition-based method for the control of shunt active filter (SAF) under balanced and unbalanced loads, which extracts fundamental components of load current and estimates the reference currents. The results show satisfactory responses, which were verified by means of simulation and prototype experimentation. Mu *et al.* [9] described a modified passivity-based control (PBC) tracking control scheme for SAPF is presented which achieves zero steady-state current error, while conventional PBC-based SAPF could not achieve it. This is experimentally demonstrated using a 380 V/75 A developed prototype. Wang *et al.* [10] presented a hybrid system, which imparts current tracking of extensive bandwidth and swift dynamic response. In order to suppress resonance and coupling between modules, a new kind of self-adaptive active damping technique is also proposed.

Yang and Yang *et al.* [11] presents a dual-loop current control method for a digitally control led LCL-type SAPF. The limitation of the damping region in the PR unit is eliminated by means of the delay-compensation control link, which improves system robustness without introducing any additional active damping loop. The results are implemented on a 30 kVA active power filter prototype. SMC has been presented with improved results when compared with the hysteresis current control [12]. Geng *et al.* [13] presented a fast repetitive control scheme with harmonic correction loops is presented for SAPF in a weak power grid, which improves dynamic performance, validated through simulation and experimentation. A fuzzy global sliding mode control method is presented for SAPF using adaptive control theory, thereby reducing the THD of source current below 5 percentage [14]. Nie and Liu [15] proposed a current reference control method is proposed for the SAPF, which utilizes the Kalman filter. Zhou *et al.* [16] suggested a unique adaptive DC-link voltage management technique for SAPF in order to lower switching noise and switching loss when the system is in operation. The real-time observer is used to record the peak grid voltage. Experiments verify the suggested method's effectiveness.

Jayasankar and Vinatha [17], using a backstepping controller, which is quick, reliable, and stable, the shortcomings of the traditional method—poor stability margin, steady state inaccuracy, and chattering issues—were solved. Static and dynamic conditions are applied to and assessed on a lab specimen. A current and energy-based time-invariant state space model with switching functions is derived as the basis of a technique [18]. Lower dc-capacitor values are used to validate the suggested technique. Komurcugil *et al.* [19] suggested a model predictive control approach based on the energy function for a single-phase, three-level T-type inverter-based SAPF, wherein the need of using a weighting factor is eliminated, which is compared with classical model predictive control (MPC) methods, and performance is validated in terms of THD of grid current on a 3 kVA system. Kurak [20] designed a proportional-integral observer (PIO) is designed for SAPF and voltage is regulated using a PI controller. Compensative current harmonics are a bit complicated using conventional SAPF, due to which Dubey *et al.* suggested a reduced order generalized integrator-based SAPF is suggested and compared for current-fed and voltage-fed non-linear loads in order to address this problem [21]. To increase load efficiency, carbon emissions from utility sectors must be decreased; that is, present harmonics that are causing system degradation must be addressed. In this context, Sant [22] suggested a dual second-order generalized integrator and least mean square based on reference current generation are suggested

for controlling the SAPF. This stops reactive current components and harmonics from entering the grid, resulting in a quicker dynamic response. A two-loop, single-phase, four-level flying capacitor multicell inverter architecture [23]. In order to create a first-order system with less peak overshoot and settling time, Hingol *et al.* suggested [24] a modified symmetrical sinusoidal integrator to pre-process supply voltages and load currents before implementing an instantaneous reactive power theory-based control of SAPF.

The basic active component of load current is computed using a moving window min-max method as the basis for the suggested SAPF control technique. The suggested strategy produces quicker, more dynamic, and more accurate steady-state responses in experimental data [25]. To lower a grid-tied inverter's THD of terminal voltage and current, Dubey *et al.* [26] suggests using a modified complex coefficient filter in a dual fundamental component extraction system to extract fundamental components for the creation of reference current. The results of this proposed dead-band elimination scheme show a significant reduction in source current harmonics validated using OPAL-RT in real-time. Different control strategies have been reviewed for shunt active filter, in which it has been portraited perfect harmonic cancellation (PHC) strategy gave better simulation results when compared to p-q and Id-Iq control strategies [27]. LQRI is proposed for LC-coupled active filter and the results obtained through simulation and experimentation justify its superior steady state performance when compared to LQR control, hysteresis current control, and proportional current control [28]. In this paper, for both state and disturbance estimation, an LQR controller, a LO, as well as UIO for SAPF, are designed. Later, a combined LQR with LO, and UIO are simulated in real-time environment through OPAL-RT.

2. MATHEMATICAL MODELING OF SHUNT ACTIVE FILTER

The dynamics of SAPF is represented in the form of three state variable equations as described in (1)-(3) [3].

$$\frac{di_d}{dt} = -\frac{R_f}{L_f}i_d + wi_q - \frac{d_d}{L_f}V_{dc} + \frac{1}{L_f}v \tag{1}$$

$$\frac{di_q}{dt} = -\frac{R_f}{L_f}i_q + wi_d - \frac{d_q}{L_f}V_{dc} \tag{2}$$

$$\frac{dV_{dc}}{dl} = \frac{3}{2C_f}\left(d_d i_d + d_q i_q\right) \tag{3}$$

Where i_d, i_q are d-q axis currents, R_f is the total losses in coupling resistance and inverter, L_f is leakage inductance of the coupling inductor, d_d and d_q are d-q axis control inputs, V_{dc} represents DC-link voltage, C_f represents DC bus capacitor. The state vector $x = \begin{bmatrix} i_d & i_q & V_{de} \end{bmatrix}^T$ represents state, and control input vector $u = \begin{bmatrix} dd & dq \end{bmatrix}^T$ represents control respectively, and ϑ represents fault. The dq-frame rotates with an angle $\theta = \omega t$ from the reference axis of abc-frame. State space equation of SAPF can be written as (4), where, $x = \begin{bmatrix} i_d & i_q & V_{dc} \end{bmatrix}^T$, $u = \begin{bmatrix} d_d & d_q \end{bmatrix}^T$.

$$\dot{x} = Ax + Bu + Ev \tag{4}$$

The state, control and disturbance matrices are:

$$A = \begin{bmatrix} -\frac{R_f}{L_f} & w & -\frac{d_d}{L_f} \\ w & -\frac{R_f}{L_f} & -\frac{d_q}{L_f} \\ \frac{3d_d}{2C_f} & \frac{3d_q}{2C_f} & 0 \end{bmatrix}, B = \begin{bmatrix} \frac{V_{dc}}{L_f} & 0 \\ 0 & \frac{V_{dc}}{L_f} \\ \frac{3I_d}{2C_f} & \frac{3I_q}{2C_f} \end{bmatrix} \text{ and } E = \begin{bmatrix} -\frac{1}{L_f} & 0 & 0 \end{bmatrix}^T$$

3. PROPOSED METHOD
3.1. LQR design for SAPF

For LQR design, [3] all the states are assumed to be available for feedback for SAPF, i.e $C = \begin{bmatrix} 1 & 0 & 0 \\ 0 & 1 & 0 \\ 0 & 0 & 1 \end{bmatrix}$. The optimal control law u= -Kx can be obtained by minimizing the cost function, as in (5).

$$J = \int_0^\infty \left(x^T Q x + u^T R\, u \right) dt \tag{5}$$

The gain matrix $K = R^{-1} B^T P$ can be obtained solving Ricatti equation, as in (6).

$$A^T P + PA - PBR^{-1} B^T P + Q = 0 \tag{6}$$

Where tuning matrices Q and R represent state and control weighing matrices which are assumed to be square and symmetric:

$$Q = \begin{bmatrix} Q_{id} & 0 & 0 \\ 0 & Q_{iq} & 0 \\ 0 & 0 & Q_{Vdc} \end{bmatrix} \text{ and } R = \begin{bmatrix} R_{id} & 0 \\ 0 & R_{iq} \end{bmatrix}$$

The initial values of Q_{id}, Q_{iq}, Q_{Vdc}, R_{id}, R_{iq} are chosen by using Bryson's rule [27], which are then further tuned until the desired performance is achieved.

3.2. Observer design for SAPF

In this section, it is assumed that all states are measurable. However, it is not always possible to measure all states. In this aspect, the observer can be used to estimate the states from a limited number of sensors. For observer design, it is assumed that the only the first state i_d is available for feedback, i.e $C_{obs} = \begin{bmatrix} 1 & 0 & 0 \end{bmatrix}$.

3.2.1. Luenberger observer based control

Figure 1 depicts the schematics of LO for SAPF. The state space model of LO-based control for SAPF is expressed as (7) and (8) [4].

$$\dot{\hat{x}} = A\hat{x} + Bu + L(y - \hat{y}) \tag{7}$$

$$y = C_{obs}\hat{x} \tag{8}$$

Where $\hat{x}$ is estimated state variables and $\hat{y}$ is estimated output. Consider the estimation error as $e = \hat{x} - x$ and its derivative is (9).

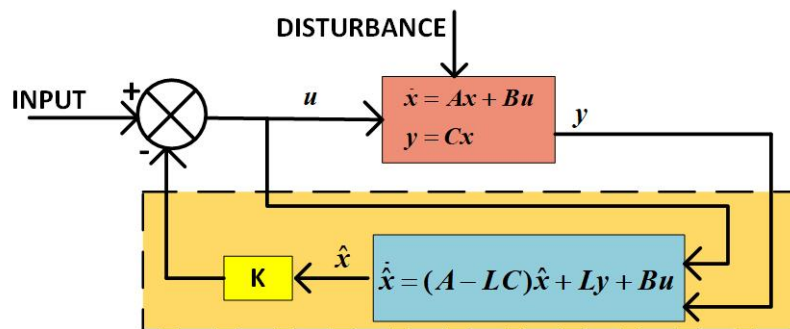$$\dot{e} = \dot{\hat{x}} - \dot{x} = (A - LC_{obs})e + Ev \tag{9}$$

Figure 1. Schematic diagram of LO with LQR for SAPF

In the absence of disturbance, the Luenberger observer can exactly estimate state variables in finite time. For appropriate design of L, $(A - LC_{obs})$ must be stable, which indicates all eigenvalues of $(A - LC_{obs})$ should have negative real parts. However, if there is a fault, there will be a steady state error between the estimated and actual state variables.

3.2.2. PI observer based control

Figure 2 depicts the schematics of PIO for SAPF. This observer has an additional degree of freedom, because of the presence of integral part. Hence, this observer improves the dynamics of estimation when compared to LO. There are two feedback loops which has to be designed, one is proportional loop and the other is integral loop. As compared to Luenberger observer, the PIO eliminates the steady state error, in the presence of disturbances [20]. PIO is designed to estimate the state and fault of LQR controlled SAPF. The state space model of PIO can be shown as:

$$\dot{\hat{x}} = (A - L_pC)\hat{x} + Bu + L_py + Ed$$
$$y = C\hat{x}$$

Consider the estimation error $\hat{e} = x - \hat{x}$. The derivative of $\hat{e}$ is:

$$\dot{\hat{e}} = \dot{x} - \dot{\hat{x}} = Ax - (A - L_pC)\hat{x} - L_py = (A - L_pC)e$$

L_p and L_I should be selected such that all the eigen values of $(A - L_pC)$ should have negative real parts. Therefore, without and with disturbance, there will be no steady state error between estimated and actual state variables in finite time. The gains L_p represents proportional gain and L_I is integral gain.
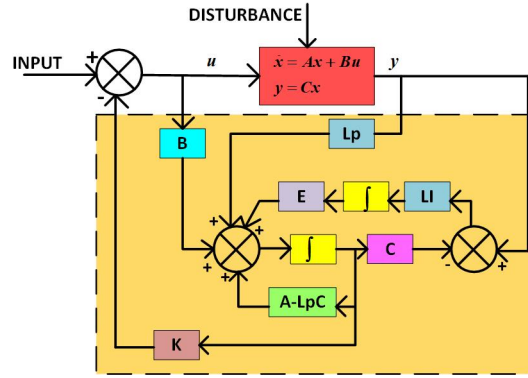

Figure 2. Schematic diagram of PIO with LQR for SAPF

3.2.3. UI observer based control

Figure 3 depicts the schematics of UIO for SAPF. The state dynamics of UIO is given by (10) and (11).

$$\dot{z}(t) = Fz(t) + TBu(t) + Ky(t) \tag{10}$$

$$\hat{x}(t) = z(t) + Hy(t) \tag{11}$$

Where $z \in \mathbb{R}^n$ is the state of full order observer, $\hat{x} \in \mathbb{R}^n$ is the state estimate and matrices F, T, K, H are designed. From the block diagram, it is obvious that UIO decouples state estimation dynamics from the disturbance term in the original system.

The following is the UIO design procedure: Figure 4 shows the flow chart depicting step by step procedure for designing UIO. Here, in (12)-(16).

$$H = E[(CE)^T CE]^{-1}(CE)^T \tag{12}$$

$$T = I - HC \tag{13}$$

$$A_1 = TA \tag{14}$$

$$F = A_1 - K_1C \tag{15}$$

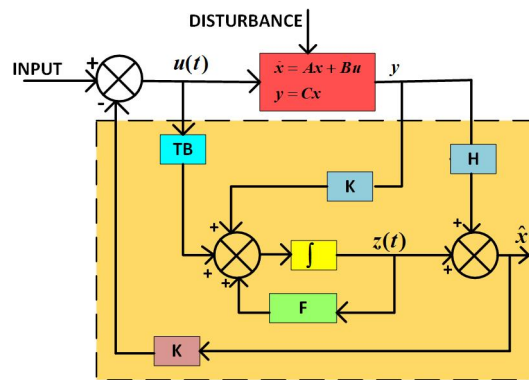$$K = K_1 + K_2 = K_1 + FH \tag{16}$$

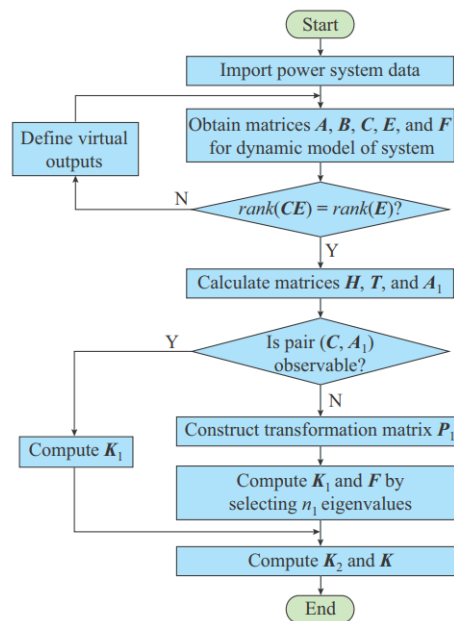Figure 3. Schematic diagram of UIO with LQR for SAPF

Figure 4. Flow chart depicting procedure of design of UIO

4. REAL-TIME SIMULATION RESULTS

The transfer function of observer controller is given by (17) and (18).

$$G_c(s) = \frac{U(s)}{-Y(s)} = [K(sI - A + K_eC + BK)^{-1}K_e]$$

$$= \frac{1155s^2 + (2.406e^8)s - (769e^9)}{s^3 + (4e^5)s^2 + 3.93e^{10} - (1.169 * e^{14})} \tag{17}$$

The transfer function of plant (SAF) is given by (18).

$$G_p(s) = \frac{3s^2 + 6100s + 3396800}{s^3 + 2000s^2 + 1098700s + 338.4} \tag{18}$$

The Bode plot diagram of open loop and closed loop system is shown in Figure 5. It can be observed from the plots that Gain margin of open loop system is $+\infty$, gain margin of closed loop system is $+\infty$ and phase margin of open loop and closed loop systems are 90 degrees and $+\infty$ respectively, which indicate the system considered along with controller and observer is stable both in open loop as well as closed loop.
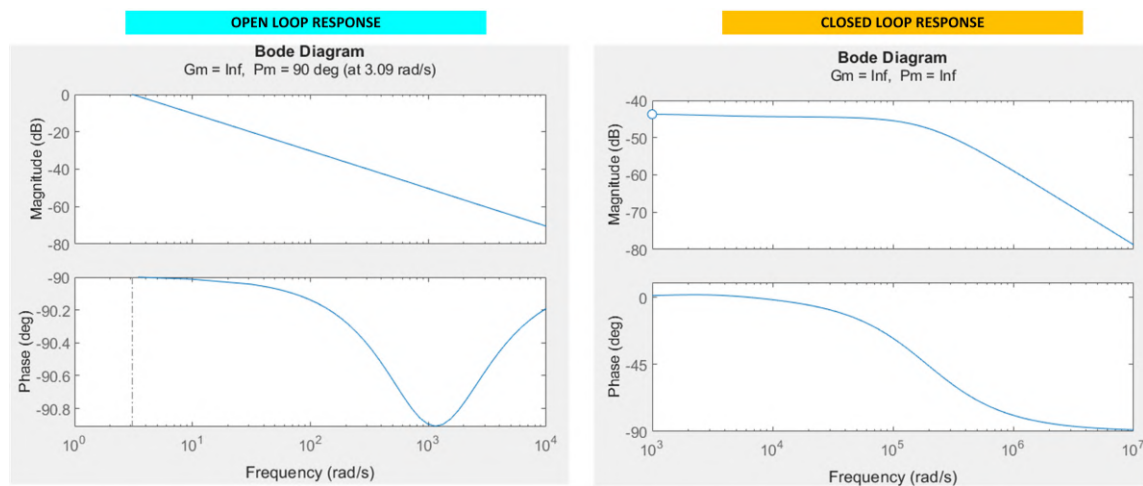
Figure 5. Bode plots of open loop and closed loop system

Figure 6 displays the features of the target computer along with the real-time simulator OP4610XG. Figure 7 displays the back view of the OP4610XG and a list of the signal conditioning modules included in the system that was supplied. The complete configuration utilizing an OPAL-RT (OP4610XG) module is shown in Figure 8. MATLAB/Simulink and OPAL-RT are often preloaded on the host device, which is a personal computer. Under dynamic operation situations, the target device (OP4610XG) generates real-time simulation results in a hardware-synchronized real-time simulation mode. First, using easily available Simulink block sets, the shunt active filter (SAF) based control and the suggested control technique are modeled in the MATLAB/Simulink environment. The simulation model is then split into two subsystems utilizing communication blocks (found in the OPAL-RT library): an optctrl, optcom, analog in, and analog out. The system model is contained in the master subsystem, whereas the console subsystem has the necessary scopes.A TCP/IP Ethernet connection cable is seen in Figure 8 and is used to facilitate communication between the host and the target devices. The relevant data is then retrieved using a USB disk that is connected into the USB ports of the Keysight Technologies DSO58, 350 MHz, 1 GS/s oscilloscope in a research simulation. The OPAL-RT simulator (OP4610XG), the host or target PC running RT-LAB software, and an Ethernet connection cable with TCP/IP make up the experimental setup. A full simulation system running on a Kintex7 FPGA is called the OP4610XG. It is made up of a signal conditioning stage, a versatile high-speed processor, and a potent target computer. Six extra input/output low voltage differential signaling (LVDS) connections are included in the system, which may be utilized in optical fiber or RS422 mode. An entry-level system with an FPGA carrier that can accommodate four standard OPAL-RT boards and two optional 6-transceiver modules is the OP4600 series hardware. It has an FPGA carrier that can accommodate two optional 6 transceiver modules in addition to four regular OPAL-RT boards. An OPAL-RT Board I/O instance is added to the RT-LAB project in order to handle I/O signals configuration settings, programming and initialization of the FPGA, and the choice of hardware synchronization mode of the card, all while utilizing OPAL-RT I/O modules with OPAL-RT Board I/O management system.

The eHSx32 solver, which has two Quadrature Encoder RS422 inputs and outputs in addition to sixteen analog outputs, thirty-two digital inputs, and thirty-two digital outputs, is used to setup the I/O. The OPAL-RT connectors 2B, 2A, 1A, and 1B, respectively, offer access to these 16 analog outputs (AOUT00 to AOUT15), 16 analog inputs, 32 digital inputs (DIN00 to DIN31), and 32-digit outputs (DOUT00 to DOUT31). The target machine must have the RT-LAB software installed. The following are the implementation procedures to obtain the real-time simulation results after launching the RT-LAB program. The new RT-Lab project option is chosen from the File menu. A project is created when the project name is provided. After creating the project in the preceding step, an existing MATLAB model has to be added. The current MATLAB model has been modified to work with OPAL-RT. Afterwards, you must choose the new RT-LAB target choice from the File Menu. In order to view the specifics of the target, such as processing speed, number of active cores, and number of kernel versions of the operating system, an IP address must be supplied. Error will appear if the target device is not connected to the host PC. When this option is chosen in RT-LAB, a number of sequential procedures will

occur, including model separation, C code generation, C code transfer, C code building, and model build and transfer. All systems/models need to be turned into subsystems in order for them to be compatible with OPAL-RT. The MATLAB file will be accessible after execution. We are able to adjust the settings as needed. The OPAL-RT results of faulty dynamics of states i_d and i_q of SAF and their estimates $\widehat{i_d}$, $\widehat{i_q}$ using LQR controller with LO, and UIO with sinusoidal input, in the presence of step disturbance and three unknown disturbances, i,e sinusoidal, triangular, and noise type are exhibited in this section.

Items	Quantity	Description
Chassis Type	1	OP4610XG
Operating System		Opal-RTLinux 3.4.1
CPU	1	CPU - AMD Ryzen 5 3600XT, 6-Core, 3.8GHz
Total Core #	6	
Memory	2	8 GB
Motherboard		X570D4U-2L2T AsRock uATX Server Motherboard, AMD socket AM4 PGA 1331 Dual 10GLAN
IP Addresses		10.64.117.188 (enp39s0) – see Figure 3 for identification
AC Input		100-240V, 60-50Hz
FPGA Board Index		00

Figure 6. OP4610XG real time simulator and features of target computer

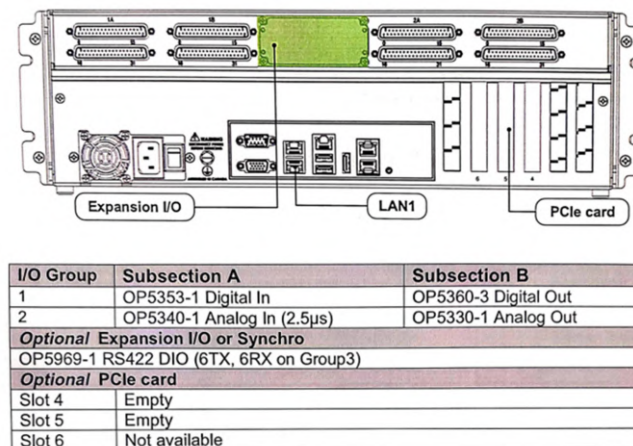| I/O Group	Subsection A	Subsection B
1	OP5353-1 Digital In	OP5360-3 Digital Out
2	OP5340-1 Analog In (2.5µs)	OP5330-1 Analog Out
Optional Expansion I/O or Synchro		
OP5969-1 RS422 DIO (6TX, 6RX on Group3)		
Optional PCIe card		
Slot 4	Empty	
Slot 5	Empty	
Slot 6	Not available	

Figure 7. OP4610XG rear view and modules of signal conditioning in delivered system
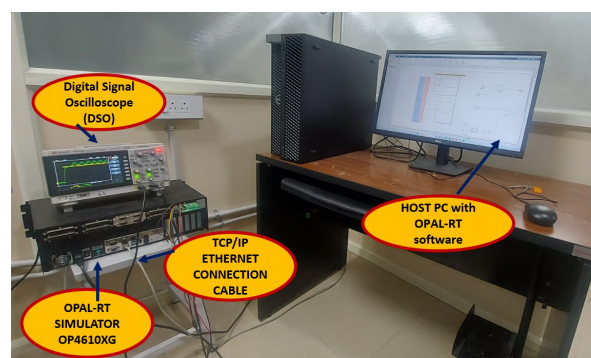

Figure 8. OPAL-RT OP4510 simulation setup in real time

4.1. LQR controller driven of SAPF with Luenberger, and UI observers-disturbance case

4.1.1. Case-1(a): Sinusoidal input in the presence of unknown disturbance1(SINUSOIDAL) using OPAL-RT OP4510

The simulation results of the disturbance dynamics of d and q axis currents of SAPF i.e i_d, i_q and their estimates $\widehat{i_d}$, $\widehat{i_q}$ using LQR controller with LO, PIO, and UIO, with sinusoidal input, in the presence of unknown sinusoidal disturbance are exhibited in Figures 9 and 10. It can be observed from Figures 9 and 10 that i_d and i_q of SAF and their estimates $\widehat{i_d}$, $\widehat{i_q}$ using LQR controller with LO and PIO in the presence of sinusoidal disturbance are not retaining the desired step reference signal. It is very obvious from the results that there exists a steady state error between actual states and estimated states (waveform in yellow color) with respect to the reference step signal (waveform in green color). However, UIO in the presence of unknown sinusoidal disturbance is retaining the also reference input.
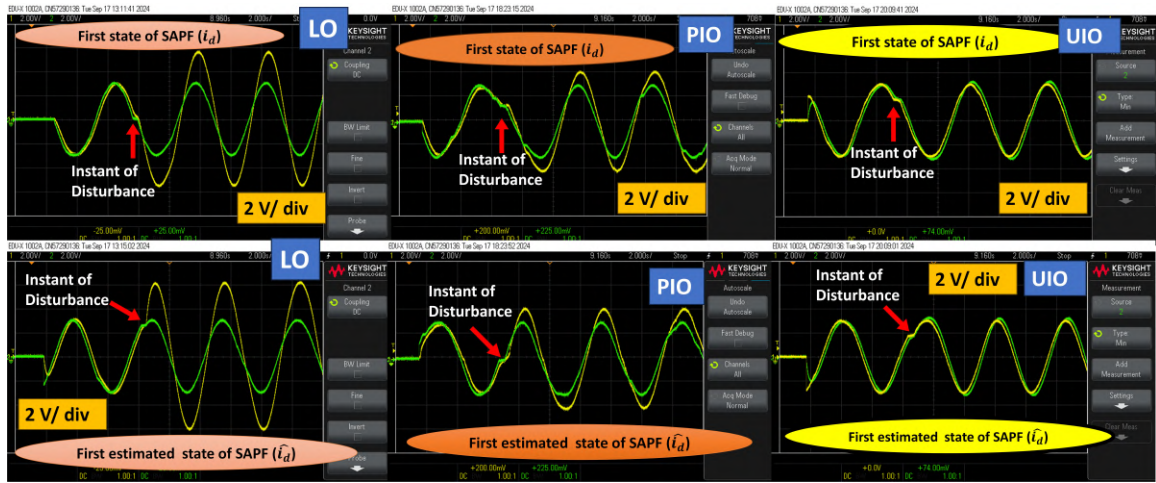

Figure 9. Tracking of first state and its estimated state of LO, PIO, and UIO-based control of SAPF under unknown sinusoidal disturbance using OPAL-RT OP4510
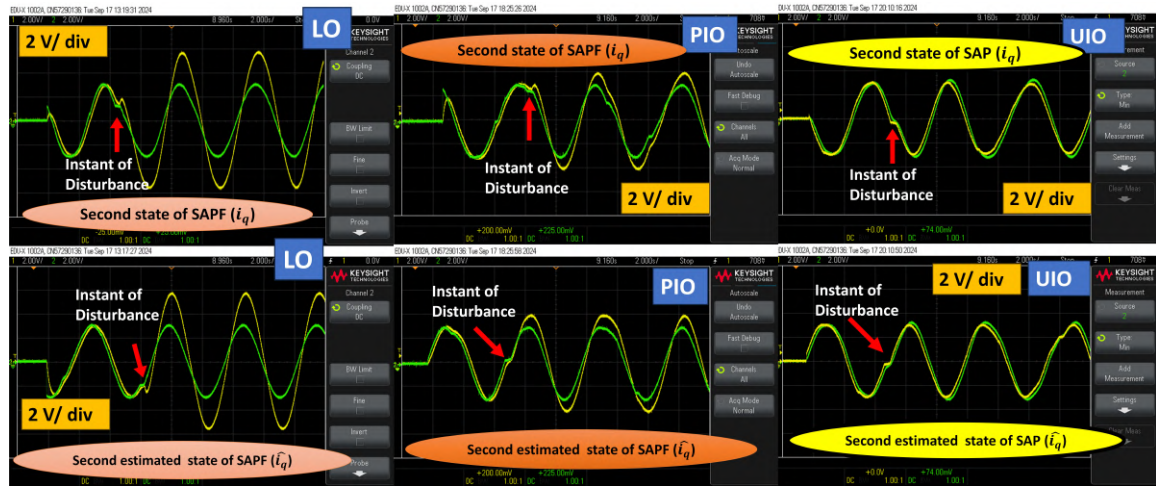

Figure 10. Tracking of second state and its estimated state of LO, PIO, and UIO-based control of SAPF under unknown sinusoidal disturbance using OPAL-RT OP4510

For additional examination, each case's inaccuracy between states and its estimate with respect to reference are taken into account. Figure 11 displays the error plots of LO, PIO, and UIO based control of SAF with unknown sinusoidal disturbance that were similarly simulated using SFB and LQR. Table 1 contains a

tabulation of the maximum and minimum range values of errors achieved with sinusoidal disturbance. It can be clearly concluded from Table 1 that error range in case of UIO-based control of SAP is very less than compared to that of LO and PIO.

Table 1. Error analysis for LO, PIO, and UIO based control of SAP in presence of unknown sinusoidal disturbance

| Case	Error taken	Error range(OPAL-RT)
$LO - LQR(SinDisturbance)$	i_d and reference	-3.03 to 3.24
$LO - LQR(SinDisturbance)$	$\widehat{i_d}$ and reference	-2.79 to 3.00
$LO - LQR(SinDisturbance)$	i_q and reference	-3.11 to 3.24
$LO - LQR(SinDisturbance)$	$\widehat{i_q}$ and reference	-2.79 to 3.08
$PIO - LQR(SinDisturbance)$	i_d and reference	-550 m to 620 m
$PIO - LQR(SinDisturbance)$	$\widehat{i_d}$ and reference	-570 m to 620 m
$PIO - LQR(SinDisturbance)$	i_q and reference	-570 m to 620 m
$PIO - LQR(SinDisturbance)$	$\widehat{i_q}$ and reference	-580 m to 670 m
$UIO - LQR(SinDisturbance)$	i_d and reference	-71 m to 78 m
$UIO - LQR(SinDisturbance)$	$\widehat{i_d}$ and reference	-71 m to 74 m
$UIO - LQR(SinDisturbance)$	i_q and reference	-67 m to 74 m
$UIO - LQR(SinDisturbance)$	$\widehat{i_q}$ and reference	-67 m to 78 m
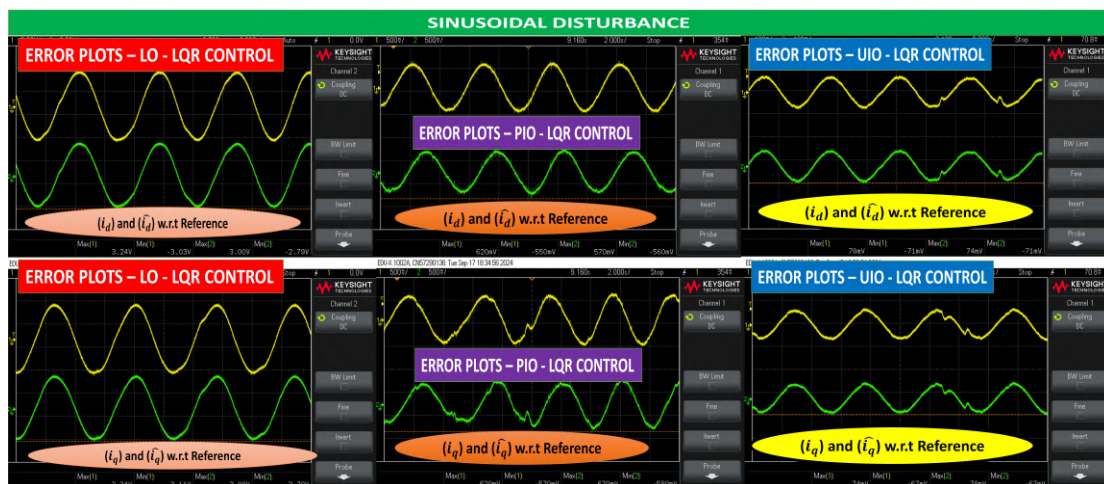
Figure 11. Error plots of actual and estimated states with LO, PIO, and, UIO in the presence of sinusoidal disturbance using OPAL-RT OP4510

4.1.2. Case-1(b): Sinusoidal input in the presence of unknown disturbance2(TRIANGULAR) using OPAL-RT OP4510

The simulation results of disturbance dynamics of d and q axis currents of SAPF i.e i_d, i_q and their estimates $\widehat{i_d}$, $\widehat{i_q}$ using LQR controller with LO, PIO and UIO, with sinusoidal input, in the presence of triangular disturbance are exhibited in Figures 12 and 13. It can be observed from Figures 12 and 13 that i_d and i_q of SAF and their estimates $\widehat{i_d}$, $\widehat{i_q}$ using LQR controller with LO and PIO in the presence of unknown disturbance2(TRIANGULAR) are not retaining the desired step reference signal. It is very obvious from the results that there exists a steady state error between actual states and estimated states (waveform in yellow color) with respect to the reference step signal (waveform in green color). For additional examination, each case's inaccuracy between states and its estimate with respect to reference are taken into account. Figure 14 displays the error plots of LO, PIO, and UIO based control of SAF with unknown sinusoidal disturbance that were similarly simulated using SFB and LQR. Table 2 contains a tabulation of the maximum and minimum range values of errors achieved with triangular disturbance. It can be clearly concluded from Table 2 that error range in case of UIO-based control of SAP is very less than compared to that of LO and PIO.

Table 2. Error analysis for LO, PIO, and UIO based control of SAP in presence of unknown triangular disturbance

| Case	Error taken	Error range(OPAL-RT)
$LO - LQR(Triangular\,Disturbance)$	i_d and reference	-140 m to 1.99
$LO - LQR(Triangular\,Disturbance)$	$\widehat{i_d}$ and reference	-210 m to 1.88
$LO - LQR(Triangular\,Disturbance)$	i_q and reference	-300 m to 1.63
$LO - LQR(Triangular\,Disturbance)$	$\widehat{i_q}$ and reference	-290 m to 1.60
$PIO - LQR(Triangular\,Disturbance)$	i_d and reference	-310 m to 360 m
$PIO - LQR(Triangular\,Disturbance)$	$\widehat{i_d}$ and reference	-320 m to 370 m
$PIO - LQR(Triangular\,Disturbance)$	i_q and reference	-350 m to 380 m
$PIO - LQR(Triangular\,Disturbance)$	$\widehat{i_q}$ and reference	-340m to 370m
$UIO - LQR(Triangular\,Disturbance)$	i_d and reference	-68 m to 73 m
$UIO - LQR(Triangular\,Disturbance)$	$\widehat{i_d}$ and reference	-63 m to 86 m
$UIO - LQR(Triangular\,Disturbance)$	i_q and Reference	-64 m to 77 m
$UIO - LQR(Triangular\,Disturbance)$	$\widehat{i_q}$ and reference	-59 m to 86 m
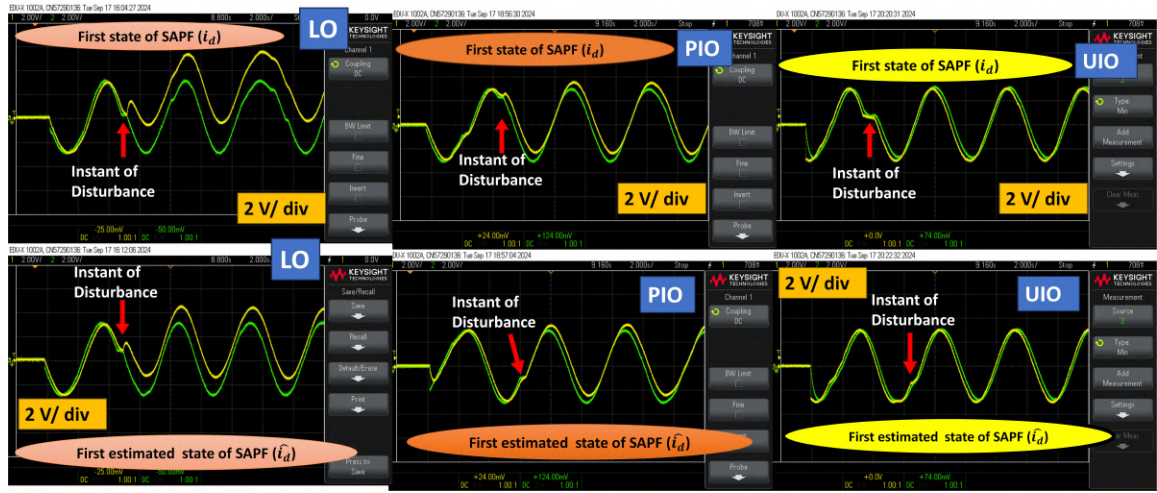
Figure 12. Tracking of first state and its estimated state of LO, PIO, and UIO-based control of SAPF under unknown triangular disturbance using OPAL-RT OP4510
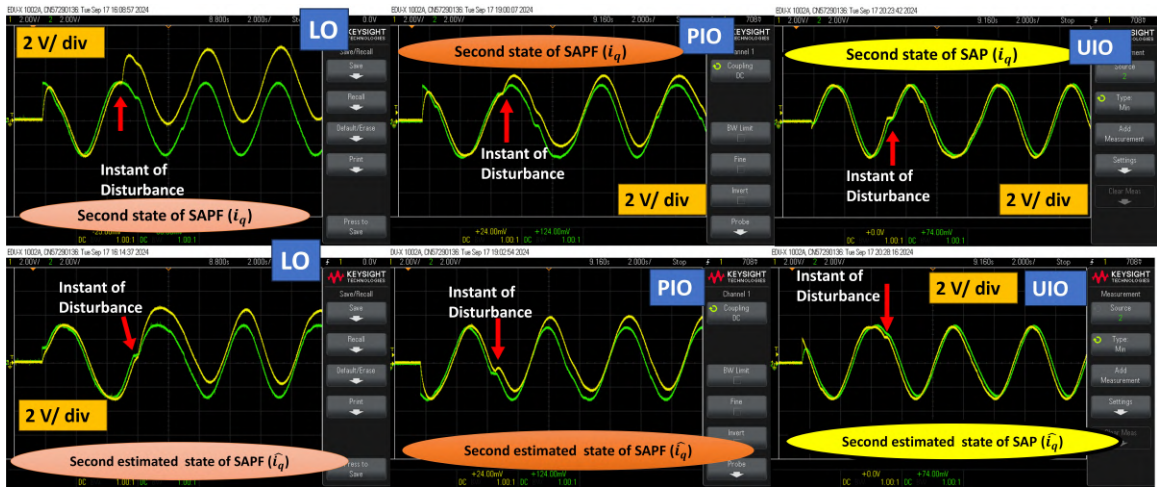

Figure 13. Tracking of second state and its estimated state of LO, PIO, and UIO-based control of SAPF under unknown triangular disturbance using OPAL-RT OP4510
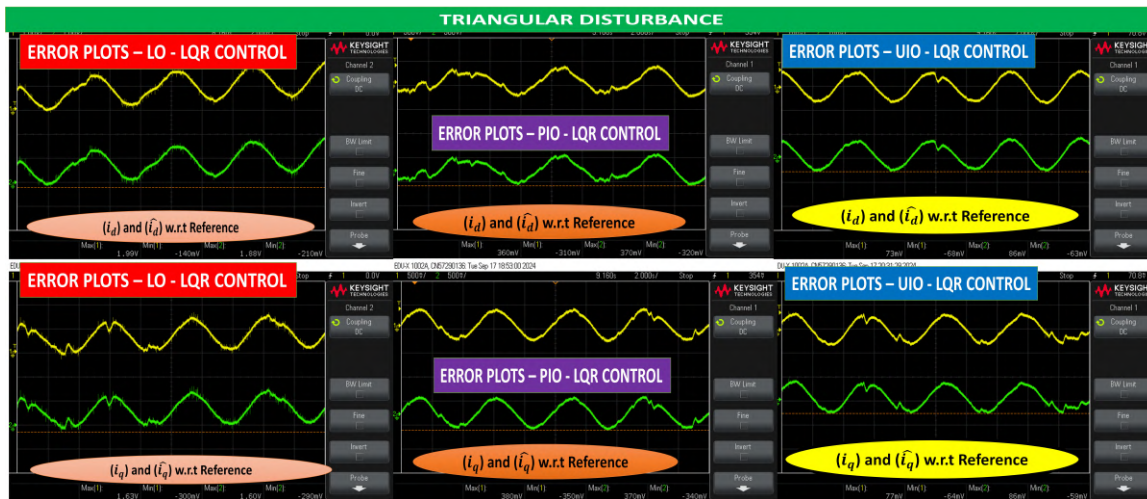
Figure 14. Error plots of actual and estimated states with LO, PIO, and UIO in the presence of triangular disturbance using OPAL-RT OP4510

4.1.3. Case-1(c): Sinusoidal input in the presence of unknown disturbance3(NOISE-TYPE) using OPAL-RT OP4510

The simulation results of disturbance dynamics of d and q axis currents of SAPF i.e i_d, i_q and their estimates $\widehat{i_d}$, $\widehat{i_q}$ using LQR controller with LO, PIO, and UIO with sinusoidal input, in the presence of noise-type disturbance are exhibited in Figures 15 and 16. On the other hand, UIO in the presence of noise-type disturbance is retaining the reference input.
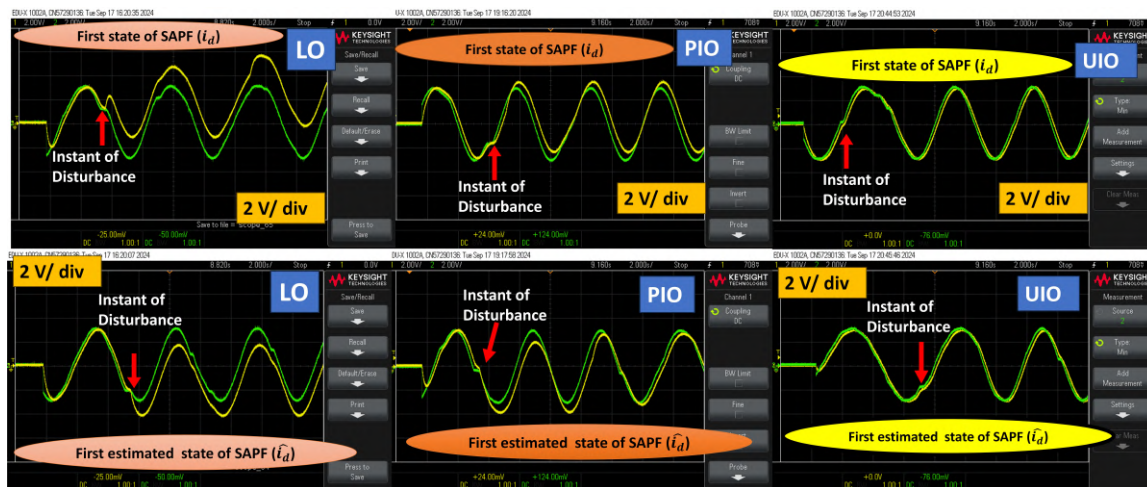
Figure 15. Tracking of first state and its estimated state of LO, PIO, and UIO-based control of SAPF under noise-type disturbance using OPAL-RT OP4510

It can be observed from Figures 15 and 16 that i_d and i_q of SAF and their estimates $\widehat{i_d}$, $\widehat{i_q}$ using LQR controller with LO and PIO in the presence of unknown disturbance3 (NOISE-TYPE) do not retain the desired step reference signal. It is very obvious from the results that there exists a steady state error between actual states and estimated states (waveform in yellow color) with respect to the reference step signal (waveform in green color). On the other hand, UIO in the presence of noise-type disturbance is retaining the also reference input. For additional examination, each case's inaccuracy between states and its estimate with respect to reference are taken into account. Figure 17 displays the error plots of LO, PIO, and UIO based control of SAF with noise-type disturbance that were similarly simulated using SFB and LQR. Table 3 contains a tabulation of the maximum and minimum range values of errors achieved with triangular disturbance. It can

be clearly concluded from Table 2 that error range in case of UIO-based control of SAP is very less than compared to that of LO and PIO.

Table 3. Error analysis for LO, PIO, and UIO based control of SAP in presence of unknown noise disturbance

| Case	Error taken	Error range(OPAL-RT)
$LO - LQR(Noise - typeDisturbance)$	i_d and reference	-1.68 to 1.69
$LO - LQR(Noise - typeDisturbance)$	$\hat{i_d}$ and Reference	-1.58 to 1.76
$LO - LQR(Noise - typeDisturbance)$	i_q and reference	-1.04 to 1.57
$LO - LQR(Noise - typeDisturbance)$	$\hat{i_q}$ and reference	-1.07 to 1.63
$PIO - LQR(Noise - typeDisturbance)$	i_d and reference	-370 m to 470 m
$PIO - LQR(Noise - typeDisturbance)$	$\hat{i_d}$ and reference	-550 m to 430 m
$PIO - LQR(Noise - typeDisturbance)$	i_q and reference	-350 m to 350 m
$PIO - LQR(Noise - typeDisturbance)$	$\hat{i_q}$ and reference	-370 m to 440 m
$UIO - LQR(Noise - typeDisturbance)$	i_d and reference	-64 m to 77 m
$UIO - LQR(Noise - typeDisturbance)$	$\hat{i_d}$ and reference	-59 m to 78 m
$UIO - LQR(Noise - typeDisturbance)$	i_q and reference	-64 m to 77 m
$UIO - LQR(Noise - typeDisturbance)$	$\hat{i_q}$ and reference	-59 m to 86 m
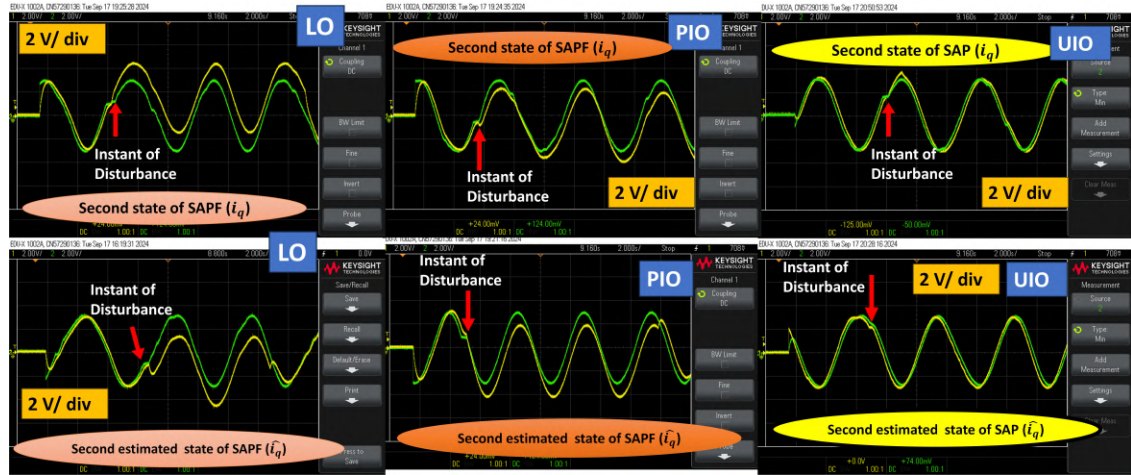
Figure 16. Tracking of second state and its estimated state of LO, PIO and UIO-based control of SAPF under noise-type disturbance using OPAL-RT OP4510
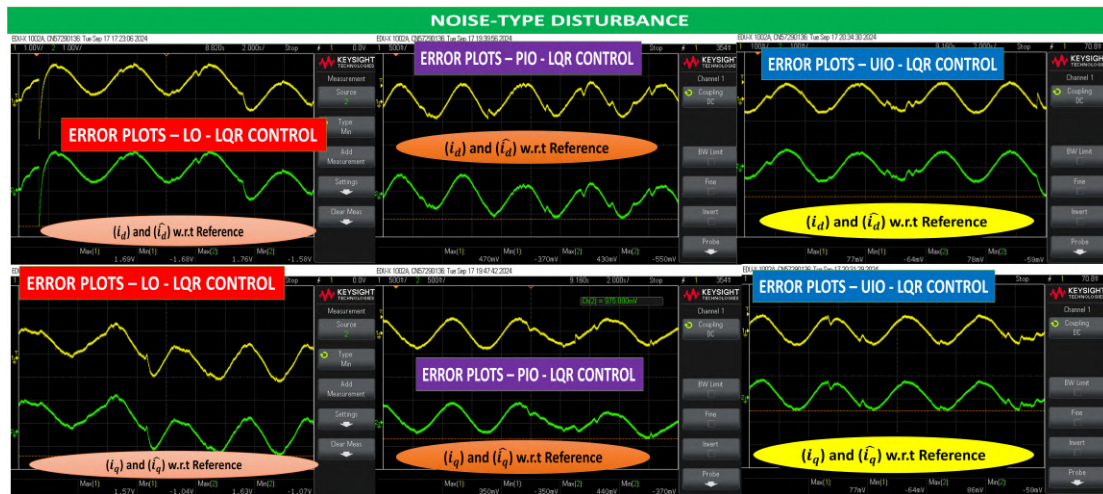

Figure 17. Error plots of actual and estimated states with LO, PIO, and UIO in the presence of triangular disturbance using OPAL-RT OP4510

Real-time implementation of a combined controller-observer approach for ... (Nagulapati Kiran)

Apart from state estimation, UIO also estimates the step disturbance and three unknown disturbances as shown in Figures 18-20. Figures 18-20 depicts the estimation of unknown sinusoidal, triangular and noise-type disturbances. The estimated disturbance state (yellow color) is perfectly tracking the actual disturbance (green color). Hence, it can be observed that UIO is perfectly tracks various disturbances that have been considered.
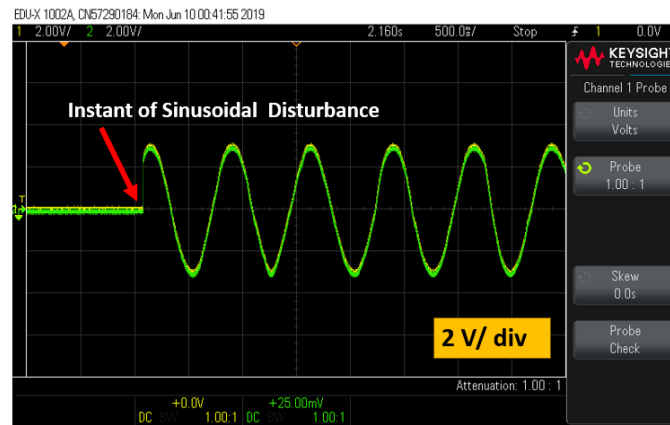

Figure 18. Sinusoidal disturbance estimation of UIO-based control of SAPF using OPAL-RT
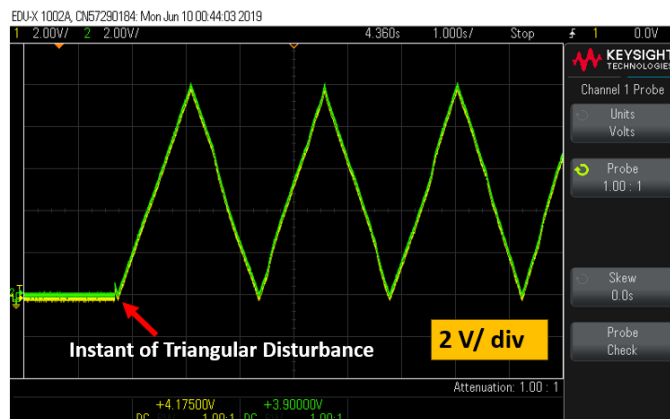
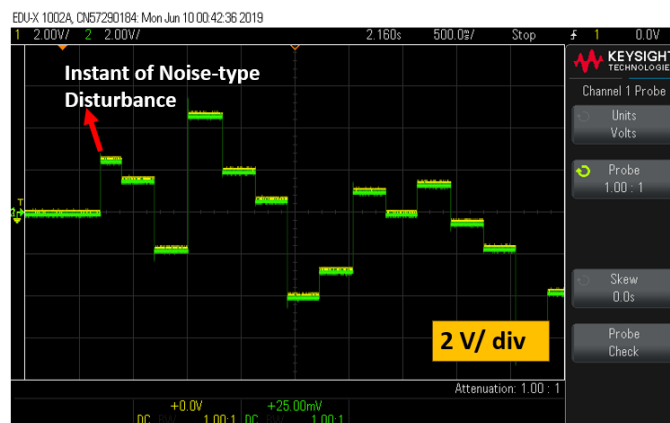Figure 19. Triangular disturbance estimation of UIO-based control of SAPF using OPAL-RT

Figure 20. Noise-type disturbance estimation of UIO-based control of SAPF using OPAL-RT

5.   CONCLUSION

In this paper, a full-state feedback controller is designed based on LQR for SAPF. To avoid this requirement of full state feedback, LO, PIO, and UIO are designed in presence of various unknown disturbances for SAPF. It can be observed from real time implementation results that in the presence of a disturbance, LO and PIo fails to track the reference sinusoidal input and it introduces a steady state error between the reference input and estimated state. UIO eliminates this steady-state error, it perfectly tracks sinusoidal reference inputs in the presence of a disturbance. Apart from state estimation, UIO also, perfectly estimates the various disturbances. Error analysis of LO, PIO, and UIO based control of SAPF in the presence of all three unknown disturbances has been simulated by OPAL-RT and data have been tabulated in addition to state and disturbance estimation. These values demonstrate that UIO is more resistant in the presence of disturbances than LO and PIO, with a smaller error range. The system under consideration is stable in both open and closed loop scenarios, as demonstrated by the subsequent derivation of the open loop and closed loop transfer functions and the plotting of the corresponding bode-plots.

REFERENCES

[1]   S. K. Jain and P. Agarwal, "Design simulation and experimental investigations, on a shunt active power filter for harmonics and reactive power compensation," *Electrical Power Components and Systems*, vol. 31, no. 7, pp. 671–692, Jul. 2003, doi: 10.1080/15325000390203674.

[2]   H. Akagi, E. H. Watanabe, and M. Aredes, "Instantaneous power theory and applications to power conditioning," New York, USA: John Wiley & Sons, 2017.

[3]   B. Kedjar and K. Al-Haddad, "DSP-based implementation of an LQR with integral action for a three-phase three-wire shunt active power filter," *IEEE Transactions on Industrial Electronics*, vol. 56, no. 8. pp. 2821-2828, Aug. 2008, doi: 10.1109/TIE.2008.2006027.

[4]   T. Jarou, E. Abderrahmane, E. Nabil, and N. Abdelhamid, "New control based on estimated state feedback of the shunt active filter to compensate for the disturbing currents in the electric power," *International Review on Modelling and Simulations (IREMOS)*, vol. 7, pp. 457-465, 2014.

[5]   M. T. Benchouia, I. Ghadbane, A. Golea, K. Srairi, and M. H. Benbouzid, "Design and implementation of sliding mode and PI controllers based control for three phase shunt active power filter," *Energy Procedia*, vol. 50, pp. 504-511, 2014, doi: 10.1016/j.egypro.2014.06.061.

[6]   M. Ali, A. Kaur, and A. H. Bhat, "Comparative analysis of shunt active filter with PI controller and ANN based controller," *International Journal of Computer Applications*, vol. 147, no. 4, pp. 1-6, Aug. 2016, doi: 10.5120/ijca2016910966.

[7]   Y. Hoon, M. A. Mohd Radzi, M. K. Hassan, and N. F. Mailah, "Control algorithms of shunt active power filter for harmonic mitigation: A review," *Energies*, vol. 10, no. 12, 2017, doi: 10.3390/en10122038.

[8]   S. Shukla, S. Mishra, B. Singh, and S. Kumar, "Implementation of empirical mode decomposition-based algorithm for shunt active filter," *IEEE Transactions on Industry Applications*, vol. 53, pp. 2392-2400, Jun. 2017, doi: 10.1109/TIA.2017.2677364.

[9]   X. Mu, J. Wang, W. Wu, and F. Blaabjerg, "A modified multi-frequency passivity-based control for shunt active power filter with model parameter adaptive capability," *IEEE Transactions on Industrial Electronics*, vol. 65, no. 1, pp. 760-769, Jan. 2018, doi: 10.1109/TIE.2017.2733428.

[10]   Y. Wang, J. Xu, L. Feng, and C. Wang, "A novel hybrid modular three-level shunt active power filter," *IEEE Transactions on Power Electronics*, vol. 33, no. 9, pp. 7591-7600, Sep. 2018, doi: 10.1109/TPEL.2017.2772811.

[11]   L. Yang and J. Yang, "A Robust dual-loop current control method with a delay compensation control link for LCL-type shunt active power filters," *IEEE Transactions on Power Electronics*, vol. 34, no. 7, pp. 6183-6199, Jul. 2019, doi: 10.1109/TPEL.2018.2865813.

[12]   I. Ullah and M. Ashraf, "Sliding mode control for performance improvement of shunt active power filter," in *SN Applied Sciences*, Switzerland AG: Springer Nature, 2019, doi: 10.1007/s42452-019-0554-9.

[13]   H. Geng, Z. Zheng, T. Zou, B. Chu, and A. Chandra, "Fast repetitive control with harmonic correction loops for shunt active power filter applied in weak grid," *IEEE Transactions on Industry Applications*, vol. 55, no. 3, pp. 3198-3206, Jun. 2019, doi: 10.1109/TIA.2019.2895570.

[14]   S. Hou, J. Fei, Y. Chu, and C. Chen, "Experimental investigation of adaptive fuzzy global sliding mode control of single-phase shunt active power filter," *IEEE Acess*, vol. 7, pp. 64442-64449, May 2019, doi: 10.1109/ACCESS.2019.2917020.

[15]   X. Nie and J. Liu, "Current reference control for shunt active power filter under unbalanced and distorted supply voltage conditions," *IEEE Access*, vol. 7, pp. 177048-177055, Dec. 2019, doi: 10.1109/ACCESS.2019.2957946.

[16]   J. Zhou, Y. Yuan, and H. Dong, "Adaptive DC-link voltage control for shunt active power filters based on model predictive control," *IEEE Access*, vol. 8, pp. 208348-208357, Nov. 2020, doi: 10.1109/ACCESS.2020.3038459.

[17]   V. N. Jayasankar and U. Vinatha, "Backstepping controller with dual self tuning filter for single-phase shunt active power filters under distorted grid voltage condition," *IEEE Transactions on industry applications*, vol. 56, no. 6, pp. 7176-7184, Dec. 2020, doi: 10.1109/TIA.2020.3025520.

[18]   H. Wang and S. Liu, "Harmonic interaction analysis of delta-connected cascaded H-bridge based shunt active power filter," *IEEE Journal of Emerging and Selected Topics in Power Electronics*, vol. 8, no. 3, pp. 2445-2460, Sep. 2020, doi: 10.1109/JESTPE.2019.2930033.

[19]   H. Komurcugil, S. Bayhan, N. Guler, and F. Blaabjerg, "An effective model predictive control method with self-balanced capacitor voltages for single-phase three-level shunt active filters," *IEEE Access*, vol. 9, pp. 103811-103821, Jul. 2021, doi: 10.1109/ACCESS.2021.3097812.

[20] S. Kurak, "Disturbance observer based control of shunt active power filter," in *Karabegović, I. (eds) New Technologies, Development and Application IV. NT 2021. Lecture Notes in Networks and Systems* New York: Springer, May 2021, pp. 549-562.

[21] A. K. Dubey, J. P. Mishra, and A. Kumar, "Comparative analysis of ROGI based shunt active power filter under current fed and voltage fed non-linear loading conditions" in *International Conference on Advances in control and optimization of dynamical systems*, vol. 55, no. 1, Feb. 2022, pp. 156-161, doi: 10.1016/j.ifacol.2022.04.026.

[22] A. V. Sant, "Shunt active power filtering with reference current generation based on dual second order generalized integrator and LMS algorithm," *Energy Reports*, vol. 8, pp. 886-893, Nov. 2022,, doi: 10.1016/j.egyr.2022.08.099

[23] C. Taghzaoui, A. Abouloifa, B. Tighazouane, E. Aicha, I. Lachkar, Y. Mchaouar, and F. Giri, "Advanced control of single-phase shunt active power filter based on flying capacitor multicell converter" *IFAC-PapersOnLine*, vol. 55, no. 12, pp. 55-60, 2022, doi: 10.1016/j.ifacol.2022.07.288.

[24] H. Hingol, V. Deshpande, and A. V. Sant, "Modified symmetrical sinusoidal integrator and instantaneous reactive power theory-based control of shunt active filter," *Energy Reports*, vol. 8, pp. 515-523, Nov. 2022, doi: 10.1016/j.egyr.2022.08.151.

[25] A. J. Patel and A. V. Sant, "Power quality enhancement for charging station with moving window min-max algorithm based shunt active power filter," *Energy Reports*, vol. 8, pp. 86-91, Dec. 2022, doi: 10.1016/j.egyr.2022.10.280.

[26] A. K. Dubey, J. P. Mishra, and A. Kumar, "Modified CCF based shunt active power filter operation with dead-band elimination for effective harmonics and unbalance compensation in the 3-phase 3-wire system," *IEEE Transactions on Power Delivery*, vol. 37, no. 3, pp. 2131-2142, Jun. 2022, doi: 10.1109/TPWRD.2021.3104828.

[27] S. Mikkili and A. Padamati, "PHC, id-iq and pq control strategies for mitigation of current harmonics in three-phase three-wire shunt active filter with pi controller," *International Journal of Emerging Electric Power Systems*, vol. 18, no. 2, p. 20160055, 2017, doi: 10.1515/ijeeps-2016-0055.

[28] Q. Hong, P. Chan, W. Sou, C. Gong, and C. Lam, "Linear quadratic regulator optimal control with integral action for LC-coupling hybrid active power filter," *Applied Science*, vol. 12, no. 19, Sep. 2022, doi: 10.3390/app12199772.

BIOGRAPHIES OF AUTHORS

Nagulapati Kiran received the B.Tech. degree in electrical and electronics engineering from Pydah College of Engineering and Technology, Visakhapatnam, Andhra Pradesh, India, in 2008 and the M.Tech. degree in power electronics and drives from SRM University, Chennai, India, in 2011. Currently, he is a research scholar in the department of Electrical, Electronics and Communication, GITAM, deemed to be university, Visakhapatnam, Andhra Pradesh, India and also working as an assistant professor in the Electrical and Electronics engineering department, Anil Neerukonda Institute of Technology and Sciences (A), Visakhapatnam, Andhra Pradesh, India. His research interests include controller and observer design of shunt and series active power filter, state and disturbance estimation. He can be contacted at email: kirannhephzibah@gmail.com.

I. E. S. Naidu served as an assistant professor in EEE Department of ANITS, STIET and GITAM. Currently, He is working as associate professor from 2008 in GITAM, Visakhapatnam campus. He acquired B.Tech. degree in EEE from JNTU Hyderabad and M.Tech. degree in Power systems from JNTU Kakinada. He has awarded Ph.D. in Electrical Engineering from Andhra University. His areas of interest include power system stability, power system security, smart, and micro grids. He can be contacted at email: ninjarap@gitam.edu.